行政院國家科學委員會專題研究計畫成果報告

新穎光電材料與奈米結構元件之研究—

總計畫：新穎光電材料與奈米結構元件之研究

計畫編號：NSC 90-2215-E-002-020

執行期限：90 年 8 月 1 日至 91 年 7 月 31 日

主持人：詹國禎　　執行機構及單位名稱：台灣大學光電所

一、中文摘要

本計畫從事新穎光電材料及奈米結構元件的研究，共有四個子計畫分別是(A)砷化銦/砷化鎵量子點(子計畫一)，(B)三氧化二鎵/氮化鎵(子計畫二)，(C)光電流雜訊(子計畫三)，(D)有機發光元件與材料(子計畫四)，對於新光電半導體材質的磊晶或薄膜成長，以及量子點、電子或光電元件的製作與光電特性量測，配合製程而完成創新而有用的元件。歷經二年的研究，對於砷化鎵量子點，氮化鎵金氧半導體(MOS)電子元件，砷化鎵的量子井紅外線檢測器的雜訊及有機發光元件之電學及光學特性，物理機制有充分的瞭解，而研發的光電材料及奈米元件也有十分良好的成果，詳細的計畫研究成果請參閱各子計畫報告。

關鍵詞：InAs 量子點，氮化鎵 MOS 電容，光電流雜訊，砷化鎵 QWIP，有機發光元件

Abstract

In this integrated research project, four subprojects were formed and carried out within two years. The major targets (goals) are to develop the novel electro-optic (EO) materials and devices which are based on III-V semiconductor compound materials and organic materials. The InAs/GaAs quantum dots and Ga_2O_3/GaN metal-oxide-semiconductor (MOS) capacitors were fabricated and characterized by the EO measuring system in subproject I and subproject II, respectively. The subproject III was to make and characterize the quantum well infrared photodetectors (QWIPs) as well as explore the origin of the noise due to the localized energy states. The organic light emitting devices (OLEDs) and related materials were studied in subproject IV. The overall results show that the novel materials and devices have been investigated and developed. The detail results could refer to the individual report of the subprojects.

Keywords: InAs quantum dot, GaN MOS, photocurrent niose, GaAs QWIP, OLED.

I. 引言

A.砷化銦/砷化鎵量子點

量子點具有三維的載子侷限及δ-能態的離散能階而可研發出 1.3 μm 高效能而在光通訊用的雷射。而砷化銦/砷化鎵量子點又可使用史傳斯基-克拉斯搭諾(Stranski-Krastanow；SK)模式的應力層磊晶成長術去成長量子點，使得量子點的研究有很快速的發展。目前已有 1.3 μm 單模而且臨界電流密度 30 A/cm^2 而且光輸出功率高達 100 mW 又可在室溫操作。可是有關高溫度特性，低臨界電流密度及高效能的 1.3 μm 單模雷射，仍未達到預期的理想效能且其物理機制未明，特別是模式切換現象，頻寬及發光效率會隨溫度而變，而且其頻寬與一般量子井相比，頻寬太寬。因此，在高品質的量子點之成長及光電特性的量測，有必要加予探討其物理機制。

本研究 (子計畫一) 是利用分子磊晶成長術，去成長高品質的砷化銦量子點，主要的方法是改變長晶方法，條件及參數，以獲得均勻，高密度，零缺陷而大小可變的量子點，並利用光譜術去研究其光電特性，決定其光學躍遷能值、能寬(linewidth)、及發光強度與溫度或激發光強度的溫度相關性，期能對於量子點內的電子能階之躍遷特性之物理機制的了解，而研發出高效能的 1.3 μm 雷射元件。

B.三氧化二鎵／氮化鎵

氮化鎵磊晶材質是可以製造高功率及高頻的快速元件而且可以在比較高的溫度下操作，主因是其具有較寬的能隙，高的電子飽和速度，高的擊潰電場(breakdown electric field)。因此，吸引相當多的專家學者從事氮化鎵的材料與元件製作之研究。爲了製造高速的電子元件如 MESFET，HEMTs，及 HFETs 之元件，需要有製程簡單而絕緣優良的絕緣層，當做閘絕緣層(gate insulator)。本子計畫是進行三氧化二鎵(Ga_2O_3)本質氧化層成長在砷化鎵上，並進行其電光特性量測，進而研製 MOS 結構的元件是研究的主要目標。

C.光電流雜訊

半導體內之反轉區域性能階常出現在能量帶溝中，其產生的原因可能來自雜質、缺陷、量子點、量子井或植入的奈米結構。這些局區的能態(localized states)會捕捉載子，且影響載子傳遞及放光或吸光之特性，因而影響光電或電子元件之效能，如何去除它並了解其機制是十分重要的。本子計畫是以光電流雜訊去研究區域性能階的光電性質。

D.有機發光元件與材料

隨著有機導體、絕緣體及半導體材料的進展，有機光電材料已可應用各式的電子或光電元件，如有機發光二極體(OLEDs)，感光二極體、光導元件、太陽電池及薄膜電晶體(TFTs)。一般而言，有機半導體之光電元件具有薄膜元件及低溫製程的特性，適用於各種基板及大面積的製作方式，與傳統無機半導體的製作方式有很明顯的不同。因此，如何研發大面積而適用於不同基材的有機光電材料與元件是很重要的研究主題。本研究是利用高真空昇華純化系統及高性能的高真空薄膜沉積系統去研發其製程，並利用電激發光或光激發光及絕對量子效率的光學量測術去對研發的有機光電半導體材料及元件作一系列性的研究。

II. 材料與方法

A.砷化銦/砷化鎵量子點

利用一部 VG-80H 氣相分子術磊晶成長系統在 n^+-GaAs(100)基座上成長量子點。運用分子遷移加強成長術(migration enhanced epitaxy)及順序性的分子束次單層（sub-monolayer）的方法去成長，長晶的條件及參數是 V/III=10，成長 InAs 量子點溫度在 500 °C，並被覆 10ML $In_{0.5}Ga_{0.5}As$ 的過成長層(overgrowth layer)，覆上砷化鎵的被蓋層(cap layer)。爲了量測量子點的大小，在被蓋層上再成長砷化銦量子點而其未成長的被蓋層，以電子顯微鏡或原子力顯微鏡觀測其幾何形貌及量子尺寸分析。光學特性分別是以光致螢光光譜術去觀測其放光的特性，且以光調制反射率光譜去量測其光調制反射率的能譜，並利用高斯一次微分曲線去吻合其譜線，以獲得其量子點內電子能階躍遷的能值及相關的信息。

B.三氧化二鎵／氮化鎵

本實驗樣品是以金氧有機化學蒸鍍(MOCVD)法在紅寶石基座上成長矽－摻雜 n-型 GaN 磊晶層，其摻雜濃度爲 $1.3x10^{17}$ cm^{-3} 而遷移率是 460 cm^2/Vs。本質性的 Ga_2O_3 薄膜是利用光電化學氧化(PEC)法在室溫下成長並經加熱在 400 °C 約一小時，以去除水分子及加強 Ga_2O_3 之分子結構。利用表面剖面測厚計測量其厚度約爲 180 nm。藉著熱蒸鍍術鍍上鋁膜爲接點或閘電極，膜厚爲 100 nm。由標準的先蝕刻術去製作 MOS 的元件，其面積約 $1.764x10^{-4}$ cm^{-2}。利用一般 C-V，G-V 及 I-V 等特性曲線量測系統，去進行室溫下的實驗量測。

C.光電流雜訊

設計以 GaAs/AlGaAs 爲主的多量子井光電感測器 (quantum well infrared photodetector, QWIP) 於射極與基極之間，而在基極與集極間加入雙位隙能壁濾波器，所形成的紅外線熱電子電晶體。利用極低雜訊的低溫電特性量測系統去量測 I-V 曲線及光電流雜訊。並利用 FTIR、PL 及拉曼光譜術去量測樣品之能階。

D.有機發光元件與材料

利用自行設計及裝置的高真空昇華純化系統，高功能性的高真空薄膜沈積系統，及一般光電子元件的基本製程設備，研製有機光電半導體的材質薄膜，並製作元件，並以電激發光(EL)，光致發光(PL)光譜及絕對量子效率量測系統，去進行光電特性的量測與分析。

IV. 結果與討論

A.砷化銦/砷化鎵量子點

利用 GS-MBE 成長砷化銦量子點，固定長晶的成長參數，而只改變其原子噴入之順序條件，樣品 S_1(In-Ga-As)及 S_2(In-As-Ga-As)，成長後量子點之表面幾何型貌如圖 1(SEM 影像)及圖 2(AFM 影像)。外觀形狀是似透鏡(lens-like)，其密度分別爲 $4.8x10^{10}$ cm^{-2}(S_1)及 $1.9x10^{10}$ cm^{-2}(S_2)。量子點體積(底直徑*高度)分別是 15x17 nm^2 及 6x24 nm^2。S_1 的密度比 S_2 的密度約增加三倍。而且比較均勻，而且 S_1 比 S_2 的平均體積要大一些，高精確度的量子尺寸大小，是需要進一步配合 EDAX 及高解析率的 TEM 去度量。

量子點內電子能階的躍遷而導至發光，是利用 PL 去量測其光譜。結果如圖 3(a)及(b)。由能譜上發現樣品 S_1 的發光強度比 S_2 要高而顯現紅位移(S_1 對 S_2 而言)，即是 S_1 的量子點密度高而且比較大(比較低的光學躍遷能值)。此結果是與 FEM 及 AFM 觀測的結果呈一致性。利用高斯曲線函數去吻合各個光學躍遷之能特徵值如表 1 所示。E_A 及 E_B 是來自不同大小的兩群量子點的基態光躍遷能值，E_C 是 InAs 的溼層(wetting layer)似量子井的光躍遷能值，而 E_D 及 E_E 則是來自被覆層(capping layer)及緩衝層(buffer layer)的砷化鎵能隙值。有關其他的詳細研究結果可請參閱子計畫一。

B.三氧化二鎵／氮化鎵

樣品設計的 Ga_2O_3/GaN MOS 元件結構圖如圖 4。利用 C-V 量測系統量測 C-V 與頻率的相關曲線如圖 5 所示，其結果顯示電荷耗盡(depletion)與疊積(accumulation)間的變遷，對於頻率之變化顯現平能帶(flatband)電壓有稍微變化。製作的 MOS 電容器，藉著 ac-電導量測系統可決定其介面的能階密度(interface-state density)。量測的 G_p/ω 與ω的頻譜受到閘極偏壓的變化如圖 6 所示。由實驗結果演釋求得 Dit 值約爲 $1.3*10^{11}$ $cm^{-2}eV^{-1}$，

而擊潰電壓強度約爲 0.5 MV/cm。

C.光電流雜訊

利用砷化鎵材質與合金，以研發紅外線熱電子電晶體元件，並藉著建立的低雜訊光電流的低溫量測系統，進行元件上射極及集極的雜訊量測及分析，結果顯示 QWIP 雜訊是由熱雜訊與電子電洞對產生與複合所產生的雜訊所組成的。而在集極上的射雜訊(shot noise)會因經能壁濾波器的穿隧機率而降低。

D.有機發光元件與材料

本子計畫發展出一創新的有機光電半導體摻雜技術，稱之爲有限摻雜源之擴散轉印法，利用此法可局部調制光電特性的特質，並發展出彩色的，任意圖案的，大面積，單層或多層異質結構有機發光元件的方法。利用研發的設備及創新之元件製程方法，製作出世界第一個可程式有機發光元件，模糊接面有機發光元件，及世界最亮的有機藍光元件。本計畫尚探索含 Furan 寡連芳香化合物及寡聚芴化合物等新穎的有機光電材料的材質特性，對於載子傳導之特性及物理機制也有極優的研究成果，並被接受發表於國際上化學快訊及美國化學學會期刊上。

V. 計畫成果檢討及自評

本總計畫之目標是探研新穎光電材料，設計及研發奈米結構的元件，分成三個研究子題計畫，分別是(A)砷化銦/砷化鎵量子點(子計畫一)，(B)三氧化二鎵/氮化鎵(子計畫二)，(C)光電流雜訊(子計畫三)，(D)有機發光元件與材料(子計畫四)。各子計畫之成果均詳述於各子計畫之成果報告內，請參閱各份報告，於此僅擇要描述。

本總計畫涵蓋之四個子計畫均是國際上相當熱門的研究領域，而且極具前瞻性的研究主題。由於整合之優點，在研究設備平台及人力資源均可提供十分良好的合作關係，對於資源之有效使用及跨領域的人力培育，提供了十分良好的環境，相信對於國內光電高科技的人力需求，會有絕對提升的優點。

本總計畫的研究結果也顯示十分豐碩，分別列舉說明如下：

A.砷化銦／砷化鎵量子點之光學性質：被光電或奈米科技的國際學術會議，邀請二次的口頭演講，另發表國際上具有 SCI 的期刊論文三篇。

B.三氧化二鎵／氮化鎵金屬氧化半導體之元件：本子計畫研究成果也發表於國際會議論文與期刊上。

C.光電流雜訊：本子計畫研究，正撰寫論文投稿到應用物理快訊雜誌上發表。

D.有機光電半導體及元件研究：本子計畫的研究成果，發表在應用物理快訊(Applied Physic Letters)計有六篇論文，數篇國內外的學術會議論文，已獲准一項專利。另外在化學快訊(Chemical Communication)及美國化學學會期刊分別各有一篇論文。

總之，由四個子計畫整合而成的總計畫，在爲期二年內，所執行的計畫研究成果，個人相信是極爲豐碩而達到原訂的目標。

致謝

本總計畫是含四個子計畫，進行爲期二年的整合型計畫，四個子計畫之計畫編號分別是 NSC90-2215-E-002-021，NSC90-2215-E-002-023，NSC90-2215-E-002-024 及 NSC90-2215-E-002-025。本計畫獲得國科會充分的經費及人力資助，特別表示致謝。

References

1. F. Heinrichsdorff, Ch. Ribbat, M. Grundmann, and D. Bimberg, Appl. Phys. Lett. **76**, 556 (2000).
2. P.B. Joyce, E.C. Le Ru, T.J. Krzyzewski, G.R. Bell, R. Murray, and T.S. Jones, Phys. Rev. B **66**, 75316 (2002).
3. L. Chu, M. Zrenner, M. Bichler, G. Böhm, and G. Abstreiter, Appl. Phys. Lett. **77**, 3944 (2000).
4. L. Chu, M. Zrenner, G. Böhm, and G. Abstreiter, Appl. Phys. Lett. **76**, 1944 (2000).
5. M. Hong, et al, , J. Vac Sci. Technol. B **18**, 1453 (2000).
6. L.H. Peng, et al, Applied physics letters, **76**, 511 (2000).
7. B.F. Levine, C.G. Bethea, G. Hasnain, V.O. Shen, E. Pelve, R.R. Abbott, and S.J. Hseih, Appl. Phys. Lett. **56**, 851, (1990).
8. C.V. Heer, *Statistical Mechanics, Kinetic Theory, and Stochastic Processes*, pp.84, Academic Press, New York, 1972.
9. C.C. Wu, S.W. Lin, C.W. Chen and J.H. Hsu, Applied Physics Letters, **80**, 1117 (2002).
10. C.C. Wu, C.W. Chen, Y.T. Lin, H.L. Yu, J.H. Hsu, T.Y. Luh, Applied Physics Letters, **79**, 3023 (2001).
11. C.C. Wu, C.W. Chen, T.Y. Cho, H.L. Yu, T.Y. Luh, Applied Physics Letters, **81**, 1570 (2002).
12. C.C. Wu, Y.T. Lin, H.H. Chiang, T.Y. Cho, C.W. Chen, K.T. Wong, Y.L. Liao, G.H. Lee, S.M. Peng, Applied Physics Letters, **81**, 577 (2002).

表一.砷化銦/砷化鎵量子點的光學躍遷能值.

Sample		Transition energy features									
		E_A	Γ_A	E_B	Γ_B	E_C	Γ_C	E_D	Γ_D	E_E	Γ_E
S_1	UE	1.15	34	1.23	42	—	—	1.50	11	1.52	4
	E	1.14	27	1.22	46	—	—	1.51	14	—	—
S_2	UE	1.19	23	1.25	51	1.40	8	1.50	11	1.52	6
	E	1.19	23	1.25	47	1.40	8	1.50	15	1.52	6

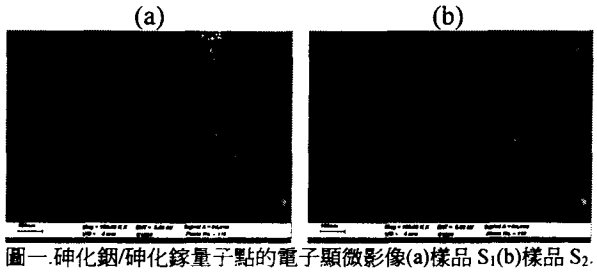

圖一.砷化銦/砷化鎵量子點的電子顯微影像(a)樣品 S_1(b)樣品 S_2.

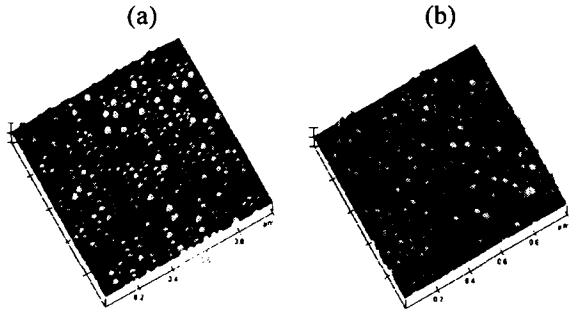

圖二.砷化銦/砷化鎵量子點的原子力影像(a)樣品 S_1(b)樣品 S_2.

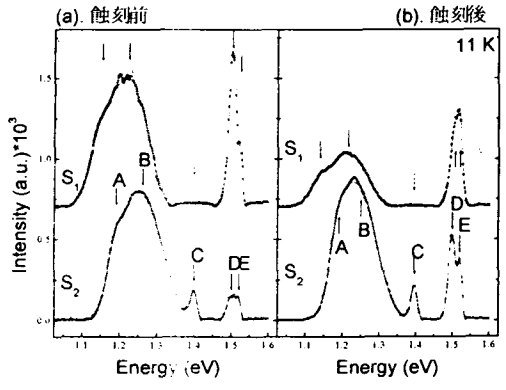

圖三.樣品 S_1 及 S_2 在 5K 溫下的光激發螢光光譜(a)樣品上層量子點未蝕除 (b)樣品上層量子點被蝕除.

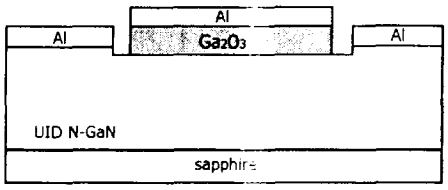

圖四.氮化鎵 MOS 結構側面圖.

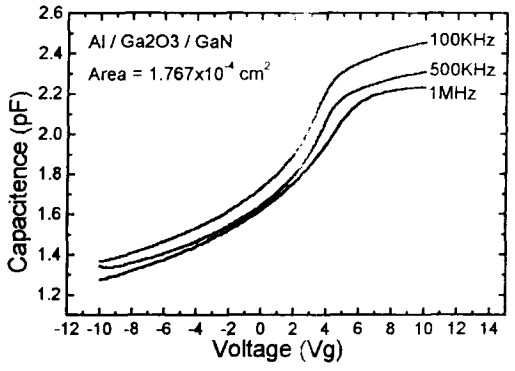

圖五.氮化鎵 MOS 頻率相關的 C-V 曲線.

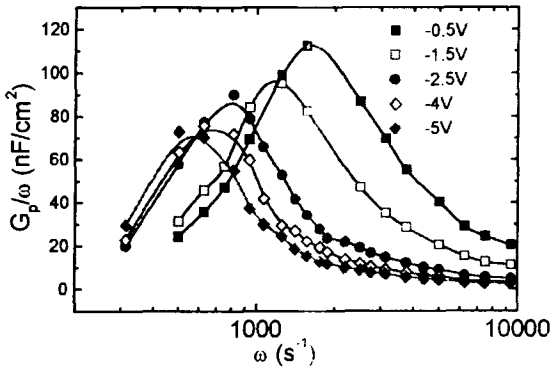

圖六.不同偏壓下對於載子耗盡區的 Gp/ω曲線.

行政院國家科學委員會專題研究計畫成果報告

新穎光電材料與奈米結構元件之研究(2/2)—

子計畫一：新穎光電材料與奈米結構元件光學性質之研究

計畫編號：NSC 90-2215-E-002-021

執行期限：90 年 8 月 1 日至 91 年 10 月 31 日

主持人：詹國禎　　執行機構及單位名稱：台灣大學光電所

共同主持人：林浩雄　　執行機構及單位名稱：台灣大學電機系

一、中文摘要

在不同溫度下，以光調制反射率光譜及光激發螢光光譜術量測砷化銦鎵/砷化鎵量子點結構的光學特性，此量子點結構樣品表面經由場發射電子掃描顯微術及原子力顯微術量測分析，其量子點面密度約為每平方公分 1×10^{10} 個。在光激發螢光光譜中顯現五個光學躍遷能譜，其中較低的兩個為量子點內能階躍遷，其次為伴隨形成之超薄量子井的躍遷，最高的兩個能階則為砷化鎵位障及緩衝層所產生。從溫度與躍遷能值關係可推論，兩個量子點的躍遷能譜的來源應是兩群由不同銦成分所構成之量子點的最低能態間光學躍遷所造成。

關鍵詞：

Abstract

The optical properties of InGaAs/GaAs quantum dots (QDs) were investigated by temperature-dependent photoluminescence (PL) and photoreflectance (PR) spectroscopies. The surface morphology and structure analysis of InGaAs QDs were also examined and characterized by a field emission scanning electron microscope (SEM) and an atomic force microscope (AFM). The area density of the QDs is on an order of magnitude about 1×10^{10} dots/cm^2. The PL results exhibited 5 major energy peaks, two of which are attributed to InGaAs QDs, one is attributed to the InGaAs wetting layer and the other two are attributed to GaAs band-gap transitions. Two of the low energy features are identified to the optical transitions of the ground state. They were originated from the two kinds of InGaAs QDs which might be formed with slight change of the indium composition. The results of PR measurements which reveal energy features on the high energy side contributed by GaAs is also reported.

Keywords: InGaAs, Quantum dots, Photoluminescence, SEM, AFM

Ⅰ. Introduction

Low dimensional semiconductor systems have been widely studied in many laboratories over the past two decades. These nanostructure materials and devices have attracted considerable attention during the last decade both from fundamental and technological points of view. Self-assembled quantum dots (QDs), one species of the nanoscale structures, provide three-dimensional confinement of the charge carriers and consequently have a discrete energy spectrum with δ-like density of states[1-2]. These zero-dimensional systems can be employed for quantum device applications such as in lasers[3], single electron transistors[4], and optical memory structures[5], which promise performance improvements of the devices compared to conventional technology. Self-assembled QDs can be formed and derived by strain in highly lattice-mismatched semiconductor materials via heteroepitaxy. The coherent islands appear beyond a critical thickness of the deposited layer during Stranski-Krastanow (SK) strained layer epitaxial growth mode[6-8]. Many workers have concentrated their efforts on the study of the structureal[9-14], optical[15-19] and electronic properties[20-22] of the InAs/GaAs self-assembled QDs. However, the overall performance of devices has remained inferior to that of quantum wells (QWs) mainly because the size, shape, and composition fluctuation that occur in QDs devices result in a broad photoluminescence (PL) line width of about 40~60 meV at room temperature.

Recently, self-assembled QDs have extended the wavelength range of the InGaAs/GaAs system further into the infrared beyond 1.3 μm[15]. The InGaAs QDs have also been optimized with uniform, homogeneous and high area densities. High-power semiconductor laser diodes based on multiple InGaAs/GaAs QDs layers grown by metal-organic chemical-vapor deposition (MOCVD) technique are demonstrated[3]. However, high quality self-assembled QDs via the Stranski-Krastanow growth mode using gas-source molecular beam epitaxy (GS-MBE) still need more work to improve their uniformly in size and shape. The identification of the growth mechanisms that lead to a narrow size distribution is of great importance.

In this work, we report growth method and parameter optimization of InGaAs/GaAs self-assembled QDs, grown by GS-MBE system using migration enhanced epitaxy technique. Optical characterization is carried out by temperature-dependent PL and photoreflectance (PR) spectroscopies. Furthermore, the morphologic and structural analyses are carried out by field emission scanning electron microscopy (SEM) and atomic force microscopy (AFM).

Ⅱ.Experimental details

The samples were grown by a VG-80H GS-MBE system on n^+-GaAs (100) substrates. Samples S_1 and S_2 were made with migration enhanced epitaxy in

a growth order sequence, In-Ga-As and In-As-Ga-As, respectively. The V/III ratio was 10 and the growth temperature was 500 °C. It consists of 500 nm of a GaAs buffer layer followed by 12 periods of GaAs/AlAs short period superlattice (SPS) with a thickness of 2 nm /2 nm, respectively. Then an undoped GaAs epilayer with a thickness of 50 nm is grown. An $In_{0.5}Ga_{0.5}As$ QD layer with a 10 monolayers (MLs) nominal thickness was grown on top of it and covered by 510 nm of GaAs. In order to examine the morphology and perform the structure analysis, the second InGaAs QDs layer was grown on the top layer.

The morphology structure and surface density analysis of InGaAs QDs on the top layer was performed with a SEM. The height and diameter of the QDs as well as size distribution were roughly measured by AFM on uncapped islands of InGaAs on the top layer. AFM measurements were carried out at ambient environment with a DI (Digital Instrument Inc.) Nanoscope III ® AFM (tapping mode).

Photoluminescence measurements were carried out with a 25-mW He-Ne laser at 632 nm and focused on to the sample to a spot size of 1 mm^2. The basic PR experimental setup is described in the literature[23]. The PR measurements were carried out with a 200-Walt halogen-tungsten lamp, which was dispersed by a monochromator to serve as a probe beam. A line of 543.2 nm He-Ne laser with output power of 100 μW was provided as a pumping beam. A mechanical chopper operated at a frequency of 265 Hz to modulate the pumping light. The optical signal of the reflected light from the sample was detected by a liquid-nitrogen-cooled InAs detector.

Ⅲ. Results and discussion

Fig. 1(a) and 1(b) show the SEM images of the InGaAs QDs for samples S_1 and S_2. The images present the uniform QDs and dome (lens-like) QD shape as well as the particle size. The area density of the QDs for S_1 and S_2 are $2.0x10^{10}$ cm^{-2} and $1.8x10^{10}$ cm^{-2}, respectively. The AFM images of samples S_1 and S_2 are shown in Fig. 2(a) and 2(b). The average of QD height and base length (diameters) for S_1 and S_2 are 15 nm × 17 nm and 6 nm × 24 nm, respectively. The area densities of the QDs for S_1 and S_2 are 4.8×10^{10} cm^{-2} and 1.9×10^{10} cm^{-2}, respectively. However, the area density of QDs is the same order of magnitude ($\sim1.0\times10^{10}$ cm^{-2}) but the magnitude is a little different. It might be due to the probing of different area of the samples using the SEM and AFM microscopes. The results confirm that the uniformity of QDs on S_1 is better than S_2, but the size of QD on S_1 is larger than S_2. It seems to be that the growth sequential ordering of In-Ga-As could improve better quality of QDs than In-As-Ga-As.

The PL spectra of un-etched samples S_1 and S_2 measured at low temperature (11 K) are shown in Fig. 3(a). Spectra at same temperature of samples S_1 and S_2 after etching the top-layer QDs are shown in Fig. 3(b).

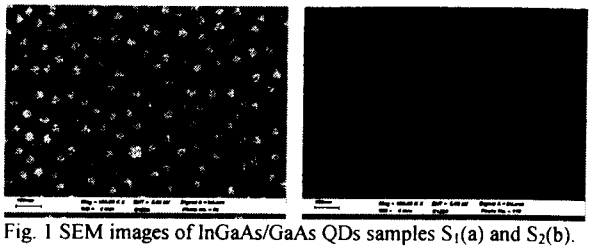

Fig. 1 SEM images of InGaAs/GaAs QDs samples S_1(a) and S_2(b).

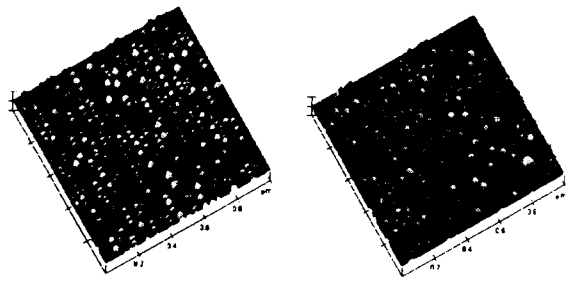

Fig. 2. AFM images of InGaAs/GaAs QDs samples S_1(a) and S_2(b).

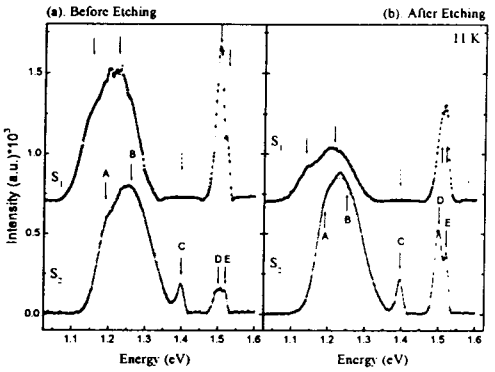

Fig. 3 Low temperature PL spectra of InGaAs/GaAs QDs with difference growth sequence ordering using migration enhanced technique for sample S_1(In-Ga-As) and S_2 (In-As-Ga-As). (a). Before removing the top QDs layer. (b). After removing the top QDs layer.

The energy features on PL for etching and un-etching cases spectra are a little different, but the major energy features are presented on both figures. The optical transitions are labeled by symbols A, B, C, D and E, and marked by arrows on peak positions shown in the figures. Before etching the top-layer QDs of sample S_1, the peak energy values E_A and E_B are 1.15 eV and 1.23 eV, respectively. The corresponding broadening parameters are 34 meV and 42 meV. After etching, the energy peak values E_A and E_B are 1.14 eV and 1.22 eV with broadening parameters 27 meV and 46 meV. The results show that the shape and particle size as well as the transition energy are slightly different. For un-etched sample S_2, the energy peak values E_A and E_B are 1.19 eV and 1.25 eV with corresponding broadening parameters 23 meV and 51 meV. After etching, the transition energy values E_A and E_B are 1.19 eV and 1.25eV with corresponding line-width parameters 23 meV and 47 meV. Unlike sample S_1, the results of S_2 show that the energy transitions and broadening parameters are almost the same. It means the growth

morphology of the QDs on top layer was less affected by the QDs grown on bottom layer covered with a 510-nm GaAs spacer. The average volume (particle size, height ×diameter^2) of the QDs on samples S_1 and S_2 measured with AFM are roughly to 4.3×10^3 nm^3 and 3.5×10^3 nm^3. Thus the average particle size on sample S_1 is larger than that on sample S_2. The results also show that transition energy of S_2 is higher than S_1. We propose that the E_A and E_B energy features are attributed to the optical transition of the ground state of the QDs with two kinds of QDs particle ensembles. The reason will be discussed in following next three paragraphs.

The energy value of the C peak is about 1.40 eV but is not present on sample S_1. It is reasonable and consistent that sample S_1 grew with higher average area density and larger average volume of the QD particles than those of sample S_2. The energy feature of the InGaAs wetting layer on InGaAs/GaAs QD specimens are reported in the literature[22]. Therefore, the E_C peak originates from the wetting layer. However, the peak disappears on sample S_1 due to the larger nano-particles (i.e. QDs). The energy value of the D and E peaks are about 1.50 eV and 1.52 eV for samples S_1 and S_2 without or with etching process. The broadening parameters are different and varied from 4 to 15 meV depending on the sample and etching process. The lower energy peak E_D (1.50 eV) is attributed to the buffer layer and the higher energy peak E_E (1.52 eV) originates from the GaAs cap layer. The fitted results are summarized and listed in Table 1.

Table 1. Summary of the fitted results from PL spectra at low temperature (11 K). Symbols are denoted with UE (un-etched) and E (etched). The transition energy values in eV and broadening parameters in meV units.

Sample		Transition energy features									
		E_A	Γ_A	E_B	Γ_B	E_C	Γ_C	E_D	Γ_D	E_E	Γ_E
S_1	UE	1.15	34	1.23	42	–	–	1.50	11	1.52	4
	E	1.14	27	1.22	46	–	–	1.51	14	–	–
S_2	UE	1.19	23	1.25	51	1.40	8	1.50	11	1.52	6
	E	1.19	23	1.25	47	1.40	8	1.50	15	1.52	6

PR spectra carried out at room temperature and low temperature are shown in Fig. 4(a) for sample S_1 and Fig. 4(b) for sample S_2 .The energy features are fitted by the third derivative function form (TDFF) with a Lorentzian line shape[24]. The energy peaks are labeled with the symbols C, D, and E corresponding to Fig. 3 and marked by an arrow notation on the peak position. Two energy values (D, E) fitted by a χ^2 fitting method of TDFF Lorentzian line shape are 1.420 (1.423) eV and 1.439 (1.440) eV at room temperature for samples S_1 (S_2), respectively. The results summary is shown in Table 2. The energy features (D, E) are attributed to the buffer and cap layers of GaAs. The peak C originates from the InGaAs wetting layer. PR spectra measured at low temperature (50 K) display more energy features which are contributed to the InGaAs wetting layer, GaAs cap and buffer layers. These energy features could not be well fitted to the room-temperature PR spectra. The line shape of PR spectra also changed severely due to temperature cooling down below 50 K. PR spectra might provide more information after detailed line shape analysis which includes strain on GaAs layer. This needs more study in the future.

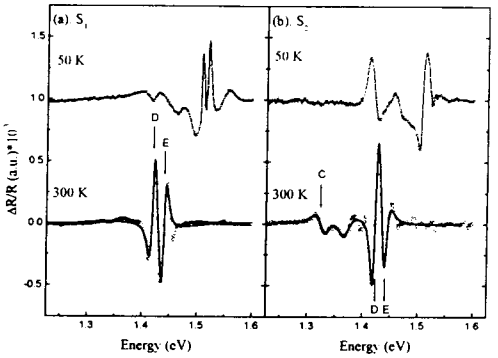

Fig. 4 PR spectra of InGaAs/GaAs QDs measured at room temperature (300 K) and low temperature (50 K) for samples (a) S_1 and (2) S_2.

Table 2. Summary of TDFF fitted results from room-temperature PR spectra of un-etched samples S_1 and S_2. Energy values in eV and broadening parameters in meV units.

Sample	Transition energy features					
	E_C	Γ_C	E_D	Γ_D	E_E	Γ_E
S_1	–	–	1.420	9	1.439	10
S_2	1.326	18	1.423	9	1.440	11

The transition energies measured with PL of low energy portions (E_A and E_B) are plotted as a function of temperature for samples S_1 and S_2 (before etching) are shown in Fig. 5. The trends observed in E_A (InGaAs QDs), E_B (InGaAs QDs) and E_C (InGaAs wetting layer) are different due to the temperature-dependent band-gap of InAs and GaAs materials. Because the wetting layer is an ultra thin InGaAs/GaAs quantum wells, the curve trend on the temperature will follow that of the host material of GaAs. However, the InGaAs QDs will be related to temperature behavior characteristic of the InAs and GaAs materials. The optical properties of the InGaAs QDs and wetting layer were studied with the fitting parameters using Varshni's equation[24]. The summary of the fitting results are listed in Table 3. The argument of the peak identification was supported by this result. A slight abnormal behavior of the inverted "S-curve" shape on temperature-dependent transition energies measured by PL spectra was observed. It has been explained by the carrier localization on potential minimum of In-rich island[24]. This effect could be studied by time-resolved PL spectroscopy in the future.

IV. Conclusion

Temperature-dependent PL and PR experiments were performed and the optical properties of Fig. 5

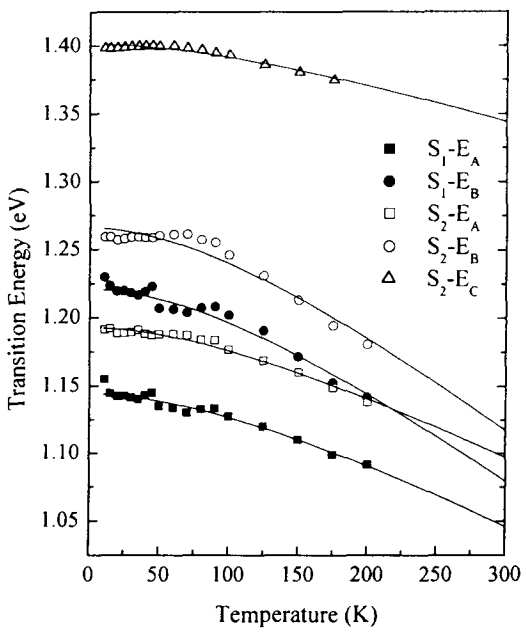

Transition energies in the low energy portion measured by PL experiments are plotted as a function of temperature.

Table 3. Results summary of the fitted parameters using Varshni's equation to fit the temperature-dependent transition energy.

Energy peak	Parameters	Sample S_1	Sample S_2	Notes
A	E (eV)	1.144	1.192	QDs[1]
	α ($\times 10^{-4}$eV/K)	-5.9	-5.8	
	β (K)	243	254	
B	E (eV)	1.221	1.266	QDs[2]
	α ($\times 10^{-4}$eV/K)	-8.7	-8.9	
	β (K)	259	245	
C	E (eV)	–	1.401	WL
	α ($\times 10^{-4}$eV/K)	–	-3.5	
	β (K)	–	253	

InGaAs/GaAs self-assembled QDs grown by GS-MBE system were studied. Samples of two growth ordering sequences of the adatom, In-Ga-As andIn-As-Ga-As, are explored and characterized with temperature-dependent transition energy spectra and identified two kinds of InGaAs/GaAs QDs ensembles which are originated from two different indium composition fluctuation. The major energy peaks display on PL and PR spectra were identified and interpreted. An abnormal behavior of the inverted "S-curve" shape presented on temperature-dependent transition energy due to carrier localization were also observed.

References

1. D. Bimberg, M. Grundmann, and N. N. Ledenstov, *Quantum Dot Heterostructures* (Wiley, Chichester, 1998).
2. Y. Toda, O. Moriwaki, M. Nishioka, and Y. Arakawa, Phys. Rev. Lett. **82**, 4114 (1999).
3. F. Heinrichsdorff, Ch. Ribbat, M. Grundmann, and D. Bimberg, Appl. Phys. Lett. **76**, 556 (2000).
4. N. Yokoyama, S. Muto, K. Imamura, M. takatsu, T.Mori, Y. Sugiyama, Y. Sakuma, H.Nakao, and T. Adachihara, Solid State Electron. 40, 505 (1996).
5. G.Yusa and H. Sakaki, Appl. Phys. Lett. 70,345 (1997).
6. I. N. Stranski and L. Krastanow, Akad. Wiss. Lit. Mainz Abh. Math. Naturwiss. **K1 IIb 146**, 797 (1939).
7. D. Leonard, K. Pond, and P. M. Petroff, Phys. Rev. B **50**, 11687 (1994).
8. D. Leonard, M. Krishnamurthy, C. M. Reaves, S. P. Denbaars, and P. M. Petroff, Appl. Phys. Lett. **63**, 3203 (1993).
9. L. Goldstein, F. Glas, J. Y. Marzin, M. N. Charasse, and G. Le Roux, Appl. Phys. Lett. **47**, 1099 (1985).
10. S. Guha, A. Madhukar, and K. C. Rajkumar, Appl. Phys. Lett. **57**, 2110 (1990).
11. J. M. Moison, F. Houzay, F. Barthe, and L. Leprince, E. Andre, and D. Vatel, Appl. Phys. Lett. **64**, 196 (1994).
12. A. Tackeuchi, Y. Nakata, S. Muto, Y. Sugiyama, T. Inata, and N. Yokoyama, Jpn. J. Appl. Phys. **34**, L 405 (1995).
13. P. B. Joyce, E. C. Le Ru, T. J. Krzyzewski, G. R. Bell, R. Murray, and T. S. Jones, Phys. Rev. B **66**, 75316 (2002).
14. A. A. Darhuber, V. Holy, J. Stangl, G. Bauer, A. Krost, F. Heinrichsdroff, M. Grundmann, D. Bimberg, V. M. Ustinov, P. S. Kop'ev, A. O. Kosogov, and P. Werner, Appl. Phys. Lett. **70**, 955 (1997).
15. R. P. Mirin, J. P. Ibbetson, K. Nishi, A. C. Gossard, and J. E. Bowers, Appl. Phys. Lett. **67**, 3795 (1995).
16. S. Farfad, R. Leon, D. Leonard, J. L. Merz, and P. M. Petroff, Phys Rev. B **52**, 5752 (1995).
17. J. M. Garcia, G. Medeiros-Ribeiro, K. Schmidt, T. Ngo, J. L. Feng, A. Lorke, J. Kotthaus, and P. M. Petroff, Appl. Phys. Lett. **71**, 2014 (1997).
18. Q. D. Zhuang, J. M. Li, H. X. Li, Y. P. Zeng, L. Pan, Y. H. Chen, M. Y. Kong, and L. Y. Lin, Appl. Pys. Lett. **73**, 3706 (1998).
19. L. Chu, M. Zrenner, M. Bichler, G. Böhm, and G. Abstreiter, Appl. Phys. Lett. **77**, 3944 (2000).
20. P. W. Fry, *et al*, Phys. Rev. Lett. **84**, 733 (2000).
21. J. J. Finley, M. Skalitz, M. Arzberger, A. Zrenner, G. Böhm and G. Abstreiter, Appl. Phys. Lett. **73**, 2618 (1998).
22. L. Chu, M. Zrenner, G. Böhm, and G. Abstreiter, Appl. Phys. Lett. **76**, 1944 (2000).
23. F. H. Pollak, in *Handbook on Semiconductors*, edited by Balhanski (North-Holland, New York, 1993), Vol. 2.
24. K. L. Teo, J. S. Colton, P. Y. Yu, E. R. Weber, M. F. Li, W. Li, K. Uchida, H. Tokunaga, N. Akutsu, and K. Matsumoto, Appl. Phys. Lett **73**, 1697 (1998).

High frequency capacitance-voltage and conductance measurement characterization of Ga_2O_3/GaN MOS

H. M. Wu (巫漢敏) and L. H. Peng
Institute of Electro-Optical Engineering,
National Taiwan University, Taipei, Taiwan, Republic of China
Rm 407, Dept. Elec. Eng.

1,Roosevelt Road, Section 4, Taipei
Tel: +886-2-2363-5251 x 407
Fax: +886-2-2367-7467
E-mail: r9941021@ee.ntu.edu.tw

Abstract: A GaN-based metal-oxide-semiconductor (MOS) structure has been fabricated by using photoelectrical-chemical technology. From the I-V measurements of the GaN-MOS, the breakdown field strength was found to be 0.5 MV/cm. The high frequency capacitance-voltage and conductance measurements revealed the interface-state density was in the range of 10^{11} cm^{-2} eV^{-1}.

NSC project code: NSC91-2622-E-002-021-CC3

1. Introduction

Gallium nitride is considered as an excellent candidate for the high-power and high frequency transistors operating at elevated temperatures, due to its wide bandgap, high electron saturation velocity, and high breakdown electrical field. Therefore the development of GaN-based transistors, including MESFETs, HEMTs, and HFETs [1]-[3] had attracted much attention, and had rapid progress in recent years. However, the excessive electrical field in the GaN substrate, surface polarization charges, and leakage current through the gate would induce the current collapse effect and limit the power-handling capabilities of these devices. Moreover when temperature raises, the gate leakage current becomes even larger, it would seriously degrade the transistor performance. By using an insulating and passivating layer under the gate electrode, it is possible to lower the gate leakage current, excessive electrical field, and surface polarization charges and to improve the device characteristics. A number of studies of the GaN metal-insulating-semiconductor (MIS) structure have been made by employing Ta_2O_5, SiO_2, Si_3N_4, and $Ga_2O_3(Gd_2O_3)$ as gate insulators [4]-[6]. But these reports showed either high leakage currents or high density of interface state. It indicated the qualities of these deposited oxide layers are not well enough for them to be gate insulator.

In this report, we present the characteristics of Ga_2O_3/GaN MOS by employing photoelectrical chemical process [7] to grow the native oxide layer Ga_2O_3 on GaN. The high frequency capacitance-voltage (C-V) and current-voltage (I-V) measurements had been taken and interface-state density was calculated by using Terman's method and conductance measurements technology.

2. Experimental

The Si-doped n-type GaN epilayers used for this report were grown on sapphire substrates by metalorganic chemical vapor deposition (MOCVD). The doping concentration and mobility are 1.3 x 10^{17} cm^{-3} and 460 cm^2/Vs, respectively.

The native Ga_2O_3 layer was grown by the PEC oxidation method at room temperature. After growth, the sample was heated up to 400°C for 1 hour to remove the H_2O molecules and strengthen the Ga_2O_3 molecular structure. The thickness of oxide layer was measured to be about 180nm by surface profiler. The metal gate and contact electrodes to the GaN substrate were made by thermal deposition of 100nm aluminum. Through standard lithography and etching process, the PEC-grown Ga_2O_3/GaN

MOS device with area 1.767×10^{-4} cm^{-2} was fabricated. Fig.1 shows the side-view structure and top-view picture of the MOS device.

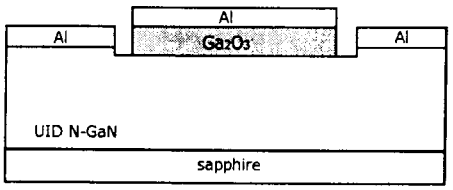

Fig.1 The side-view profile of GaN MOS.

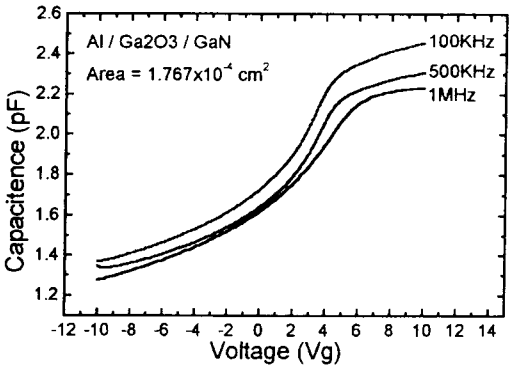

Fig.2 The C-V curves for a GaN MOS under frequency from 100k Hz to 1M Hz.

The C-V, and G-V characteristics were taken in a shielding box at room temperature using a parallel circuit model with a HP 4284 LCR meter. The I-V measurement was carried out by using a Keithley model K238 current source.

3. Results and discussion

C-V measurements for a Ga_2O_3 film 180nm-thick as grew on GaN, shown in Fig. 2, indicate a transition between accumulation and depletion, and minor shift in the flatband voltage with various frequencies. Instead of inversion, deep depletion can be reached under negative biasing voltage, indicating the generation rate of minority carriers near the surface is not sufficient to from an inversion layer. The increasing in capacitance at the accumulation with decreasing frequency is caused by the series resistance attributed to the not-perfect ohmic contact and GaN semiconductor resistance. In Fig. 3, the C-V measurements with biasing voltages sweeping up and down show a capacitance hysteresis, and indicate there are oxide traps within the Ga_2O_3 film. In the first time sweeping up to accumulation, the oxide traps catch the negative charges to become oxide-trapped charges. More positive voltage is necessary to be applied to compensate the negative oxide-trapped charges; therefore about 3V shift in curves is observed in the followed C-V sweeping measurements. From the curve-shift, the density of the oxide traps could be calculated to be $2.6\times10^{11}cm^{-2}$

In the studies of MOS capacitor, interface-state density is one of the most important parameters to confirm the quality of the interface between oxide and semiconductor layer. The most often used technology to measure the density is the Terman's method. But Terman's method grossly underestimates the actual interface-state density. Therefore we applied the ac-conductance measurement technology to more accurately probe the interface-state density [8]. The interface-state density is determined from the peak G_p/ω value, and each value of applied gate bias is converted into a surface potential corresponding to the femi-level position within the bandgap. Fig.4 shows the G_p/ω curves at different bias value corresponding to the depletion region for a GaN MOS capacitor under room temperature.

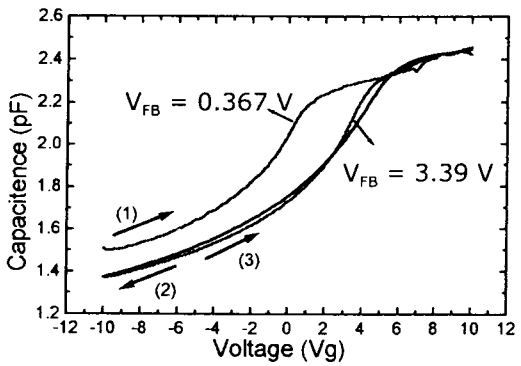

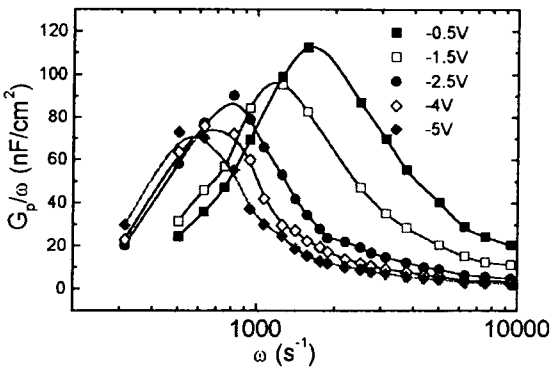

Fig. 3 The C-V traces under 1MHz with biasing voltages sweeping up(1), down(2), and up(3).

Fig. 4 The G_p/ω curves at different bias value corresponding to the depletion region for a GaN MOS capacitor.

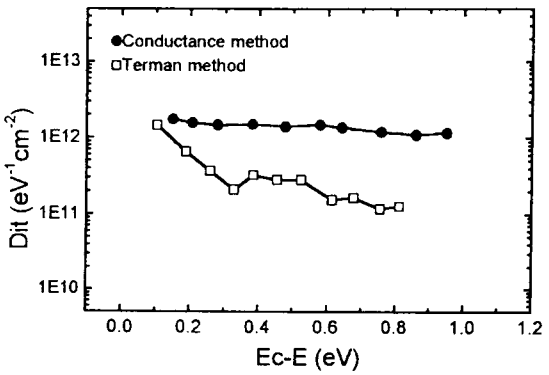

Fig. 5 Derived values of Dit as a function of energy obtained from Terman's and ac-conductance method

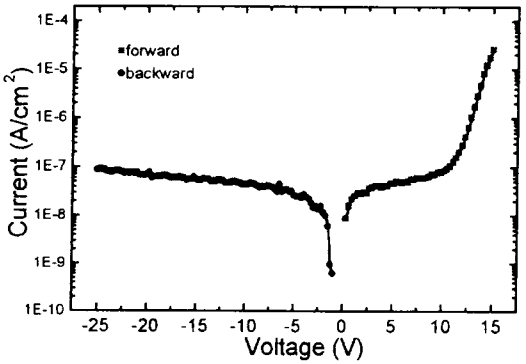

Fig. 6 gate-leakage current density vs bias voltages for GaN MOS

From the curves in Fig. 5, we are able to observe the derived values of Dit as a function of energy obtained from Terman's and ac-conductance method. As predicted, the density of Dit derived by Terman's method is smaller than that derived by ac-conductance measurement. After comparison, we can conclude the interface-state density of the Ga_2O_3/GaN MOS is in the range of 10^{11} cm^{-2} eV^{-1}, and the best result is 1.3×10^{11} cm^{-2} eV^{-1}

I-V measurements on the Ga_2O_3/GaN MOS in Fig. 6 show leakage current density in the range of 10^{-7}-10^{-9} A/cm^2, which is quite small, even at large negative biasing voltage. The derived breakdown field strength of the Ga_2O_3 oxide is about 0.5 MV/cm.

4. Conclusion

Instead of ordinary deposited insulating layer, we employed the photoelectrical chemical process to grow the native oxide Ga_2O_3 of ,GaN to be the insulating-oxide layer for MOS capacitor. We performed the Terman's and ac-conductance method to measure the interface-state density on GaN MOS capacitor. Our result shows the Dit to be in the range of 10^{11} cm^{-2} eV^{-1}, and the best result is 1.3×10^{11} cm^{-2} eV^{-1}. In addition, we examined both the leakage current and breakdown field strength, the result shows the leakage current density is quite small even at large negative biasing voltage, and the breakdown field strength of the Ga_2O_3 oxide is about 0.5 MV/cm.

5. Acknowledgment

This research is sponsored by the NSC grant No. NSC91-2622-E-002-021-CC3.

5. References

[1] W. S. Lee, et al, "high temperature performance of recessed gate GaN MESFETs fabricated using photoelectrochemical etching process", Electronics letters, vol. 36, pp. 265, 2000

[2] B. Luo, et al, "dc and rf performance of proton-irradiated AlGaN/GaN high electron mobility transistors". Applied physics letters, vol. 79, pp. 2196, 2001.

[3] X. Hu, et al, "Si_3N_4/AlGaN/GaN-metal-insulator-semiconductor heterostructure field-effect transistors". Applied physics letters, vol. 79, pp. 2832, 2001.

[4] L. W. Tu, et al, "high-dielectric-constant Ta_2O_5/n-GaN metal-oxide-semiconductor structure", Applied physics letters, vol. 77, pp. 3788, 2000.

[5] S. Arulkumaran, et al, "investigations of SiO_2/n-GaN and Si_3N_4/n-GaN insulator-semiconductor interfaces with low interface state density", Applied physics letters, vol. 73, pp. 809, 1998.

[6] M. Hong, et al, "Properties of $Ga_2O_3(Gd_2O_3)$/GaN metal-insulator-semiconductor diodes ", J. Vac Sci. Technol. B 18, pp. 1453, 2000.

[7] L. H. Peng, et al, "photoenhanced wet oxidation of Gallium nitride", Applied physics letters, vol. 76, pp. 511, 2000.

[8] MOS Physics and Technology, by E. H. Nicollian and J. R. Brews

行政院國家科學委員會專題研究計畫執行進度報告

利用光電流雜訊來研究區域性能階的光電特性
Study on Optoelectronic Properties of Localized States with Photocurrent Noise

子計畫三、

計畫編號：NSC 90-2215-E-002-024
執行期限：90/8/1~91/7/31

主持人： 管傑雄副教授　　台灣大學電機系

一、中文摘要

在本子計畫中，我們將發展光電流雜訊的量測技術來研究這些區域性能階的光電特性；尤其是它們對導電帶電子及價電帶電洞等生命期的影響。這些參數是設計雷射及偵檢器等元件的重要參數。單靠簡單的I-V或光譜量測是無法得知生命期的大小；但它們卻反應在光電流的雜訊上。由量測元件光電流的雜訊功率，求其與$4eI_{ph}$(I_{ph}為光電流)的比值，可得到雜訊電流增益。該值為載子生命期與過渡時間之比。過渡時間為載子經過樣本所需的時間，可以藉由改變樣本大小或外加電壓值而調整。如此由雜訊電流增益所求得生命期的最小值，可以不受限於儀器的頻率分析能力，此為整套系統最大的優點。

本子計畫預計以二年的時間持續發展此光電流雜訊量測技術，所針對的元件分別為GaN bulk、量子井及點、具有C-base的奈微米結構。其中的GaN bulk是研究其雜質或者是defects所造成的區域性能階；而其他的則是結構所導致的區域性能階。除了量測光電流雜訊外，我們也將針對各元件進行FTIR紅外線吸收光譜實驗、photoluminescence實驗、拉曼吸收光譜實驗、以及step scan FTIR發射光譜實驗。綜合各實驗所得的結果，以便瞭解生命期中radiative transition與nonradiative transition的相對大小，以及造成nonradiative transition的主要原因。在未來的計畫中，我們將沿用這些成果，持續發展利用奈微米結構所設計出的光電元件。

關鍵詞：區域性能階、奈微米結構、量子井、量子點、雜訊量測

二、英文摘要

In this proposal, we will develop a technique to measure the noise power of the photocurrent to investigate the localized states. In particular, the associated lifetime of the free carriers with the localized states is our primary interest. The carrier lifetime is an important parameter for those devices such as laser diodes and detectors. With simple measurement of I-V characteristics or absorption spectrum, we can not determine its value. However, it can be derived from the noise power of the photocurrent in the devices. The ratio of the photocurrent noise power over $4eI_{ph}$ where I_{ph} is the photocurrent gives the noise current gain. The noise current gain also equals the ratio of the lifetime over the transit time. In average, a free carrier passes through the sample in a transit time. Its magnitude may be changed with the sample length or the applied voltage. Therefore, the lifetime measured with the photocurrent noise is not limited by the frequency capability of the measurement system. This is the best advantage of this method to measure the carrier lifetime.

In the future three years, we will keep going on the development of the measurement technique of the photocurrent noise. The devices we will investigate are

involved with the GaN bulk, quantum wells, quantum dots, or C-base nanostructures. For the GaN bulk, we will study the localized states caused by the impurities and defects while for the others, the localized states by the nanostructures. In addition to the noise measurement, we will also proceed the measurements of the FTIR absorption spectrum, photoluminescence, Raman absorption spectrum, and step scan radiation spectrum. Based on all the experimental results, the lifetime can be analyzed for which of the radiative or nonradiative transitions is more important. In particular, the mechanism rendering the nonradiative transition is our primary concern. In the future plan, all of the results derived from this proposal will be utilized to design the optoelectronic devices with such nanostructures.

Keywords: localized state, nanostructure, quantum well, quantum dot, noise measurement.

三、計畫緣由與目的

半導體中之區域性能階常出現在能量帶溝中，其所產生的原因可起源於雜質、defect、量子井、量子點、甚至是植入的奈微米結構。這些能階會補捉導電帶的電子或價電帶的電洞，因而影響半導體的載子傳遞及放光吸光特性，若能藉用它們的影響，則可設計製作出更多具有變異性的光電元件，例如雷射、光偵檢器等。

四、執行進度

The noise characteristics are an important factor to determine the performance of an infrared photodetector, especially the noise equivalent differential temperature and the detectivity. In this paper, we report the 77K noise characteristics of an infrared hot-electron transistor (IHET) whose sample structure is shown in Fig. 1. The IHET contains a multiple quantum well photodetector (QWIP) between the emitter and the base, and a double barrier energy filter between the base and the collector.

In the noise measurement, the QWIP is under a fixed bias V_{BE} while the base and the collector are kept at the same ground potential (see Fig.1). The background noise from the measurement set-up is well calibrated and subtracted to get the noise power from the IHET. The emitter noise power (S_E) measured from the emitter current (I_E) represents the noise characteristics of the QWIP structure. The collector noise power (S_C) measured from the collector current (I_C) is the noise behavior of hot electrons injected from the QWIP and tunneling through the energy filter. The solid circles in Fig. 2 and 3 are the experimental results of S_E and S_C respectively. In addition, we also measure the dark currents (I_E and I_C), the emitter photocurrent gain g and the emitter differential conductance G at 77K.

At 77K, the dominant current in the QWIP is due to the electrons excited by thermally assisted tunneling. These electrons, travelling above the barriers and scattered by phonons or impurities, are finally trapped into another quantum well. The noise due to the thermal excitation and the trapping by quantum wells is similar to the generation-recombination noise (G-R noise) in the photoconductor. The noise power due to this mechanism[1] can be written as $4egI_E$. The reason we use the photocurrent gain is because the thermal excitation is similar to the photon excitation. The dash-dot line in Fig. 2 is the G-R noise power. Besides, the scattering process is also a noise source which is similar to the thermal noise in a conductor. This thermal noise power is 4kTG and also shown as dashed line in Fig. 2. Suppose the thermal noise and the G-R noise are independent. The sum of these two noise power is shown as the solid curve in Fig. 2 and agrees well with the experimental data. At low biases, the

thermal noise is dominant since the electric field within the barriers is weak and the current gain is small. When the bias is larger than 2.5V, the G-R noise becomes more important.

In the collector, the shot noise power, $2eI_C$, is estimated and compared with the experimental data. They agree with each other very well up to V_{BE} = 5V. According to binomial statistics, if the probability when an event occurs is much less than 1, the variance, σ^2, of the number of the event is equal to its average number.[2] Suppose the event is the tunneling of the injected hot electrons through the energy filter. Assume the minimum measurement time is τ and the average number of the tunneling electrons within τ is N. The relation between N and I_C is $I_C = eN/\tau$. Then the noise power is $e^2\sigma^2/(B\tau^2) = 2eI_C$ where $B=1/(2\tau)$ is measurement bandwidth. We also measure the transfer ratio α ($= I_C/I_E$) and find $\alpha < 0.04$ up to V_{BE} = 5V. This confirms that the tunneling probability is small and the collector noise is a shot noise.

In summary, we measure and study the emitter and collector noise of an IHET, and find that the QWIP noise can be described as the sum of the thermal noise and G-R noise while the collector noise is a shot noise when the tunneling probability through the energy filter is much less than 1.

五、圖表及註解

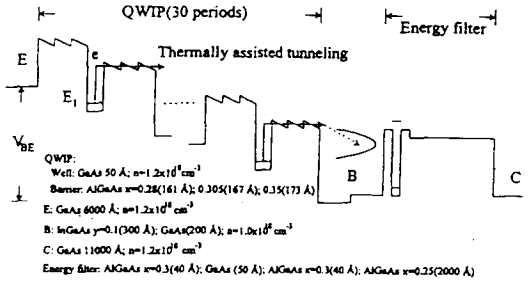

Fig. 1 The sample struccure of the infrared hot-electron transistor and its band diagram under a fixed bias VBE.

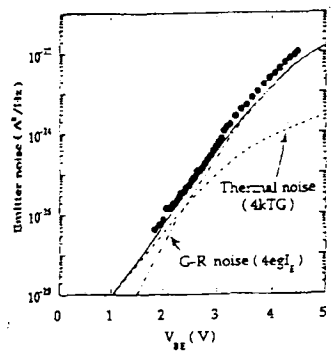

Fig. 2 Emitter noise power (solid circles) versus V_{BE}. The dash-dot line is the estimatedgeneration-recombination noise power and the dashed line is the thermal noise power. Thesolid line is the sum of the two noise powers.

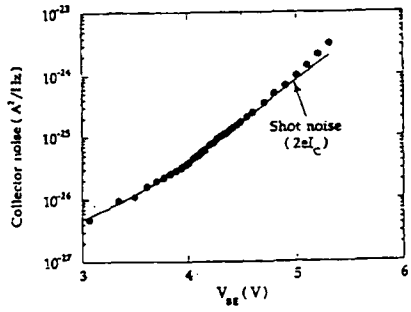

Fig. 3 Collector noise power (solid circles) versus V_{BE}. The solid line is the estimated shot noise power.

六、參考文獻

1. B. F. Levine, C. G. Bethea, G. Hasnain, V. O. Shen, E. Pelve, R. R. Abbott, and S. J. Hseih, Appl. Phys. Lett. 56, 851, (1990).
2. C. V. Heer, *Statistical Mechanics, Kinetic Theory, and Stochastic Processes*, P.84~P.86, Academic Press, New York, 1972.

行政院國家科學委員會補助專題研究計畫成果報告

※※※※※※※※※※※※※※※※※※※※※※※※※
※ 新穎光電材料及奈米結構元件之研究 ※
※ 子計畫四：有機光電半導體及元件研究(1/2,2/2)
※
※ ※
※※※※※※※※※※※※※※※※※※※※※※※※※

計畫類別：□個別型計畫 V整合型計畫

計畫編號：NSC 89－2215－E－002－049－

NSC 90—2215—E—002—025—

執行期間： 89 年 08 月 01 日 至 91 年 07 月 31 日

計畫主持人：吳忠幟

共同主持人：

本成果報告包括以下應繳交之附件：

□赴國外出差或研習心得報告一份

□赴大陸地區出差或研習心得報告一份

□出席國際學術會議心得報告及發表之論文各一份

□國際合作研究計畫國外研究報告書一份

執行單位：國立台灣大學光電工程研究所

中 華 民 國 91 年 10 月 31 日

行政院國家科學委員會專題研究計畫成果報告

新穎光電材料及奈米結構元件之研究

子計畫四：有機光電半導體及元件研究(1/2,2/2)
Studies of Organic Semiconductors and Optoelectronics

計畫編號：NSC 89-2215-E-002-049, NSC 90-2215-E-002-025
執行期限：89 年 8 月 1 日至 91 年 7 月 31 日
主持人：　吳忠幟
國立台灣大學光電工程研究所
計畫參與人員：陳介偉、林舜文、張興華、林于庭、洪文誼
莊儼郁、江獲先、卓庭毅
國立台灣大學光電工程研究所

一、中文摘要

近年來，有機半導體材料在電子及光電元件的領域裡，逐漸展現實用化的潛力。有機光電材料與元件的發展至今始進入初期的應用階段，所以無論是在元件製程、元件物理、新材料的開發以至應用的技術上，均蘊含許多發明與創新的機會，為一豐富、前瞻之研究領域。本計畫主要的目的即是針對這些重要的議題進行研究，以達到製作高功能性有機光電元件的目的。

關鍵詞：有機光電半導體；有機光電半導體元件；有機發光二極體

Abstract

With the rapid progress of organic semiconductors in recent years, organic semiconductor optoelectronics have demonstrated great potential of practical applications. Because the applications of organic optoelectronics are still in a beginning stage, there are still plenty of opportunities of invention and innovation in devices, materials and processing techniques. Therefore, the purpose of this project is to study these issues. The goal is to use these understandings in the fabrication of highly functional organic optoelectronic devices

Keywords: Organic Semiconductors, Organic Optoelectronic Devices, Organic LEDs

二、緣由與目的

近年來，隨著有機導體、絕緣體、及半導體材料的進展，有機光電材料已應用在各式電子及光電元件裡，例如有機發光二極體 (organic light-emitting diodes)、感光二極體 (photodiodes)、光導元件 (photoconductors)、太陽能電池 (solar cells)、及薄膜電晶體 (thin film transistors, TFTs)。一般而言，有機半導體光電元件具有薄膜元件及低溫製程的特性，適用於各種基板以及大面積的製作方式，將產生許多與傳統無機半導體有明顯區隔之應用，如大面積或中小型用量極大之光電系統等。本計畫近二年來，致力於新興之有機光電材料與元件(organic optoelectronic materials and devices)以及與大面積光電系統(large-area electro-optical system)，如平面顯示器，相關之光電材料、薄膜元件與應用技術課題等之研究。以下就本計畫主要的研究工作與成果作分類摘要說明。

三、結果與討論

I. 建立有機光電材料與元件研究相關設施

我們先後建立了各式有機光電材料與元件研究所需之製程與光電特性量測設施。製程方面包括：高真空昇華純化系統、高功能性之高真空薄膜沉積系統、與元件的基本製程。在材料及元件光電特性量測方面，則已建立包括：(1)電激發光(Electroluminescence, EL)相關量測設施；(2)有機薄膜或固態材料之光致發光（PL）及絕對量子效率(thin-film PL quantum yield)量測系統，我們相信這是國內第一套相關量測系統；(3)有機薄膜或固態材料之飛行時間法(Time-of-Flight)載子移動率量測系統，相信亦是國內少數常態運作之相關量測系統；(4)材料與元件之感光特性(photoresponse)量測系統。這些設施的建立，允許我們對有機光電材料、薄膜及元件特性作深度而廣泛的探討，並使得不同領域之同仁得以進行跨領域合作研究。

II. 新穎之有機光電半導體及元件製程及應用

近來我們發展出一新式有機光電半導體摻雜技術，我們稱之為有限摻雜源之擴散熱轉印法 (Finite-source dye-diffusion thermal transfer，FS-D2T2)，透過圖案化的熱轉印源，可對已形成之有機半導體薄膜進行局部的摻雜，達到局部調制光電特性的目的。利用有限摻雜源之擴散熱轉印法(FS-D2T2)可局部調制光電特性的特質，我們發展出製作彩色的、任意圖案的、大面積、單層或多層異質結構有機發光元件的方法。此外，我們進一步發現此技術可用以控制摻雜物在有機半導體薄膜之縱深分佈以優化或調制元件之各項光電特性。另外，為了降低此項製程所需之溫度，增加熱轉印之效率，我們進一步提出利用有機蒸汽輔助之有限摻雜源之擴散熱轉印法，以增進此法之應用範圍及熱轉印之解析度。同時，應用 Fick's 擴散理論，我們發展出一簡單之有限摻雜源之擴散熱轉印模型，得以相當準確分析、預測及事先設計在不同條件下之熱轉印結果與摻雜物分佈等。相關的結果我們已連續發表於三篇 Applied Physics Letters (APL)期刊論文及數篇國內外學術會議論文，已獲准一項專利，並獲邀至學術會議作邀請演講（Invited Talk)。(**參考文獻 [1]-[3]**)

III. 高性能或功能性之異質結構有機發光元件

利用不同性質有機半導體材料層，透過高度控制之高真空沈積系統，形成各種形式之有機半導體異質結構，我們藉以研究其中之各種物理機制及據以研製高性能或功能性之有機光電元件。

(1)世界第一個可程式化有機發光元件 (Programmable Organic Light-Emitting Device)

例如最近我們在 Applied Physics Letters (APL)期刊上發表了世界上第一個所謂的可程式化之有機發光元件 (Programmable OLEDs)。由於不同之有機材料具有不同的相變溫度，我們發現在適當的材料及元件結構搭配下，有機薄膜發光元件可具有可程式化的特性與功能。當我們對元件通以高電流或加熱時，使元件溫度達至某些材料層之相變溫度時，可引起元件結構性之改變，從而改變元件之操作特性及機制等。例如在我們所報導的可程式化之有機發光元件中，我們即是應用其中一電荷載子攔截材料層(carrier blocking layer)同時作為程式化時之可犧牲熔接層(sacrificial fusing layer)，在程式化過程中用以橋接兩側之材料層，使電荷載子攔截功能喪失，元件之發光顏色由原來之藍色材料層特性轉變為綠色材料層特性，而且轉變後之元件仍為正常工作的元件。利用此種元件可程式化之特性，控制元件局部之溫度可局部改變元件發光顏色，據以產生多色、圖案化之元件。此種可程式化元件或可應用於彩色 OLED 顯示器、非揮發性光學記憶元件、使用者可自行設定光色圖案之顯示商品等。此項發明與技術在 APL 揭露後，獲得多家國際科技

雜誌新聞部門之注意及詢問，目前已獲國際光學工程學會(International Society for Optical Engineering, SPIE) OE Magazine 報導為值得特別注意及觀察之光電元件及顯示器技術。（**參考文獻 [4]**）

(2)模糊接面有機發光元件 (Fuzzy-Junction Organic Light-Emitting Device)：能量使用效率最高之綠光螢光元件

目前典型之有機發光二極體之元件結構，是分別將具有電洞傳導特性、發光特性及電子傳導特性之非晶態有機材料薄膜依序沈積在已鍍有 ITO 透明電極（陽極）之玻璃基板上，最後再鍍上金屬電極（陰極）。由於各種不同的有機材料是依次沈積而形成元件，再加上有機材料間分子能階及傳導特性的不匹配，所以在兩種不同有機材料薄膜之間的介面，會形成遽變異質接面（abrupt hetero junction）。這樣的接面可以使得電子和電洞被侷限在此遽變異質接面附近，電子和電洞之濃度提高，而使得元件之發光量子效率提升。但是另一方面，也是由於遽變異質接面，使正負載子不易注入到遽變異質接面另一側之有機層，而在接面附近造成高濃度空間電荷（space charge）的累積，易形成局部的高電場，因此對元件之操作電壓上升以及元件壽命有不利之影響。因而我們發明一種新型的有機漸變接面（Organic fuzzy junction）發光元件。利用在玻璃轉換溫度（Glass transition temperature, T_g）較高的有機材料之間加入一層玻璃轉換溫度較其他材料層低的有機材料作為接面熔接層（interfacial fusing layer），當元件內部溫度高於接面熔接層之玻璃轉換溫度時，接面熔接層會引發材料間的交互擴散（interdiffusion），進而造成漸變的有機接面（fuzzy junction）。利用此漸變有機接面所製作出的有機發光二極體元件，可降低元件操作電壓同時發光效率也大幅提昇，因此元件的在相同亮度之下所消耗的能量也就大幅的下降。例如利用此種技術，我們在 Applied Physics Letters 上發表了世界上能量使用效率最高(20 lm/W)之有機螢光綠光元件。同時已申請一項專利。(**參考文獻 [5]**)

(3)世界最亮之有機藍光元件

利用我們所架設之有機薄膜之光致發光（PL）絕對量子效率(thin-film PL quantum yield)量測系統，我們發現一系列之新型藍光有機光電材料：含嘧啶環(pyrimidine)之寡連芳香化合物(Aromatic oligomer)，具有非常高之固態 PL 量子效率(>80%)，可說是有機藍光材料少見的記錄。在針對材料特性進行適當的元件結構設計，我們成功地製作出高效率以及高直流操作亮度（80000 cd/m^2）之藍光元件，是有機藍光元件僅見的紀錄。此項結果我們已發表於 Applied Physics Letters 及期刊 Organics Letters 等。(**參考文獻 [6-8]**)

IV. 新型有機光電材料之探索與光電性質研究

有機光電材料一項迷人的特點即是透過有機合成，可產生無窮盡的新材料組合及隨之無窮盡可能的性質，而這些新材料的潛力與適當應用需要仔細的光電量測與光電元件試驗加以發掘。透過與化學合成教授的合作，我們不斷探索各種新型有機光電材料，而對這些新穎材料性質的探索也常帶給我們意想不到的有趣光電性質與元件應用。

(1)含 Furan 寡連芳香化合物(Aromatic oligomer)：具有最高電洞遷移率之非芳香胺類化合物

而另外一系列的含 Furan 寡連芳香化合物(Aromatic oligomer)，利用我們所架設的 TOF 載子移動率量測系統，我們發現具有非常良好之電洞傳導特性及超過 10^{-3} cm^2/Vs 之電洞移動率(hole transport mobility)，可在有機發光元件中用為高性能之電洞傳導層材料。由於目前大部分之有機發光元件電洞傳導層材料幾全為芳香胺類分子，因此此類新型電洞傳導材料與

分子之意義與重要性不言可喻。此項的結果，目前已申請一項專利，初步元件應用結果已為期刊 Chemical Communication 接受發表，而系列性分子之 TOF 載子移動率特性及在元件中之傳導特性亦整理投稿至國際期刊。(**參考文獻 [9-10]**)

(2)寡聚芴化合物(Fluorene Oligomers)：效率最高之非摻雜藍光元件

利用我們所架設之有機薄膜之光致發光 (PL) 絕對量子效率(thin-film PL quantum yield)量測系統，我們發現一系列之新型藍光有機光電材料：寡聚芴化合物(Fluorene Oligomers)，具有非常高之固態 PL 量子效率(>80%)，同時具有良好之電荷傳遞特性，可在元件中同時扮演電荷傳遞及發光之角色。在針對材料特性進行適當的元件結構設計，我們成功地製作出不需摻雜之高效率藍光元件(3-4%)，是無摻雜藍光元件的紀錄，可大幅簡化元件之製作。此項結果我們已為期刊 Journal of the American Chemical Society 接受發表。(**參考文獻 [11]**)

四、計畫成果自評

本計畫之執行產生以下主要的成果及貢獻：

1. 建立國內第一套有機薄膜之發光量子效率量測系統。
2. 建立有機薄膜之載子遷移率率量測系統，為國內少數能常態運作之相關系統。
3. 發明有機光電半導體之新式摻雜技術：有限摻雜源之擴散熱轉印技術。
4. 發明世界上第一個可程式化之有機發光元件。
5. 發明模糊接面之有機發光元件，並用以製作具有最高能量使用效率之綠色螢光元件。
6. 研製世界最亮之有機藍光元件。
7. 共同發現數種新型及高性能之有機光電材料。
8. 發表超過十篇之國際期刊論文，部分研究成果並獲國際新聞報導 (**參考文獻 [1-11]**)。
9. 申請國內外專利四項 (**參考文獻 [18-21]**)。
10. 培養具有相關專業之碩博士生六位 (**參考文獻 [12-17]**)。

五、參考文獻

[1] C.C. Wu, C. Yang, H.H. Chang, C.W. Chen and C.C. Lee, August, 2000, "Finite-source dye-diffusion thermal transfer for doping and color integration of organic light emitting devices," *Applied Physics Letters*, Vol. 77, pp. 794-796

[2] H.H. Chang, C.C. Wu, C. Yang, C.W. Chen and C.C. Lee, February, 2001, "Graded doping profiles for reduction of carrier trapping effect in organic light emitting devices incorporating doped polymers," *Applied Physics Letters*, Vol. **78**, pp. 574-576

[3] C.C. Wu, S.W. Lin, C.W. Chen and J.H. Hsu, February, 2002, "Solvent-assisted dye-diffusion thermal transfer for electronic imaging applications," *Applied Physics Letters*, Vol. **80**, pp. 1117-1119

[4] C.C. Wu, C.W. Chen, Y.T. Lin, H.L. Yu, J.H. Hsu, T.Y. Luh, November, 2001, "Programmable organic light-emitting devices," *Applied Physics Letters*, Vol. **79**, pp. 3023-3025

[5] C.C. Wu, C.W. Chen, T.Y. Cho, H.L. Yu, T.Y. Luh, August, 2002, "Fuzzy-junction organic light-emitting devices," *Applied Physics Letters*, Vol. **81**, pp. 1570-1572

[6] C.C. Wu, Y.T. Lin, H.H. Chiang, T.Y. Cho, C.W. Chen, K.T. Wong, Y.L. Liao, G.H. Lee, S.M. Peng, July, 2002, "Highly bright blue organic light-emitting devices using spirobifluorene-cored conjugated compounds," *Applied Physics Letters*, Vol. **81**, pp. 577-579

[7] K-T. Wong, T.S. Hung, Y.-T. Lin, C.C. Wu, G.-H. Lee, S.-M. Peng, C.H. Chou and Y.O. Su, January, 2002, "Suzuki coupling approach for the synthesis of phenylene-pyrimidine alternating oligomers for blue light-emitting material," *Organic Letters*, Vol. **4**, No. 4, pp. 513-514

[8] C.F. Yang, H.D. Chen, K.H. Yang, M.K. Leung, C.C. Wu, C. Yang, C.C. Wang, W.S. Fann, August, 2001, "Synthesis and characterization of poly(2,2'-diphenylbiphenyl-4,4'-ylenevinylene-2",5"-bis(trimethylsilyl)-*para*- phenylenevinylene), a new efficient blue light-emitting polymer," *Material Science and Engineering B*, Vol. **B85**, pp. 236-241

[9] L.-Z. Zhang, C.-W. Chen, C.-F. Lee, C.C. Wu, and T.-Y. Luh, 2002, "Non-amine-based

furan-containing oligoaryls as efficient hole transporting materials," *Chemical Communication*, in press

[10] C. C. Wu, W. Y. Hung, T. L. Liu, L. Z. Zhang, T. Y. Luh, 2002, "Hole transport properties of a furan-containing oligoaryl," Journal of Applied Physics, submitted

[11] K.-T. Wong, Y.-Y. Chien, R.-T. Chen, C.-F. Wang, Y.-T. Lin, H.-H. Chiang, P.-Y. Hsieh, C.-C. Wu, C.-H. Chou, Y. O. Su, G.-H. Lee and S.-M. Peng, 2002, "Ter(9,9-diarylfluorene)s: highly efficient blue emitter with promising electrochemical and thermal stability," *Journal of the American Chemical Society*, Vol. **124**, No. 39, pp. 11576-11577

[12] 羊振中碩士論文, "Studies of finite-source dye diffusion thermal transfer for doping of organic light emitting devices", June, 2000

[13] 林舜文碩士論文, "Doping of polymer films and its applications to organic LEDs", June, 2001

[14] 陳介偉碩士論文, "Programmable heterostructure organic LEDs", June, 2001

[15] 張興華博士論文, "Doping in polymers for organic light-emitting Diodes", June 2001

[16] 江獲先碩士論文, "Optical Modeling and Analysis of Organic Light-Emitting Devices", June, 2002

[17] 莊儼郁碩士論文, "Room-temperature processed organic thin-film transistors", June 2002

[18] 吳忠幟、羊振中、張興華、陳介偉，「有限攪雜源之擴散熱轉印法」，中華民國專利，發明第 153985 號 (2002)

[19] T.-Y. Luh, L.-Z. Chang, J.-F. Lee, C.-W. Chen, C.-C. Wu, "Furan-containing hole transporting materials," 美國專利申請，application # 60/404,090, Aug. 16, 2002

[20] 吳忠幟、陳介偉、卓庭毅、陸天堯，「有機漸變接面之製造方法」，中華民國專利，申請案號 91118651 (2002)

[21] 汪根木叢，吳忠幟，「具有芳香環取代基之寡聚芴化合物」，中華民國專利申請 (2002)